ACS Catalysis

pubs.acs.org/acscatalysis

Research Article

CrO_x-Mediated Performance Enhancement of Ni/NiO-Mg:$SrTiO_3$ in Photocatalytic Water Splitting

Kai Han, Diane M. Haiber, Julius Knöppel, Caroline Lievens, Serhiy Cherevko, Peter Crozier, Guido Mul,* and Bastian Mei*

Cite This: *ACS Catal.* 2021, 11, 11049–11058

Read Online

ACCESS | Metrics & More | Article Recommendations | Supporting Information

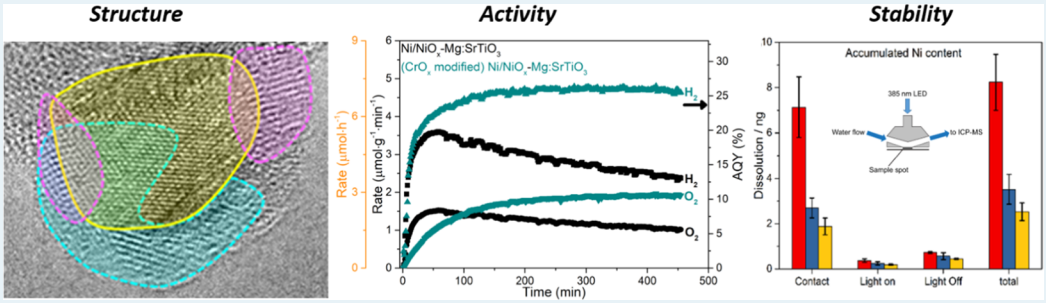

ABSTRACT: By photodeposition of CrO_x on $SrTiO_3$-based semiconductors doped with aliovalent Mg(II) and functionalized with Ni/NiO_x catalytic nanoparticles (economically significantly more viable than commonly used Rh catalysts), an increase in apparent quantum yield (AQYs) from ∼10 to 26% in overall water splitting was obtained. More importantly, deposition of CrO_x also significantly enhances the stability of Ni/NiO nanoparticles in the production of hydrogen, allowing sustained operation, even in intermittent cycles of illumination. *In situ* elemental analysis of the water constituents during or after photocatalysis by inductively coupled plasma mass spectrometry/optical emission spectrometry shows that after CrO_x deposition, dissolution of Ni ions from Ni/NiO_x-Mg:$SrTiO_3$ is significantly suppressed, in agreement with the stabilizing effect observed, when both Mg dopant and CrO_x are present. State-of-the-art electron microscopy and energy-dispersive X-ray spectroscopy (EDX) and electron energy-loss spectroscopy (EELS) analyses demonstrate that upon preparation, CrO_x is photodeposited in the vicinity of several, but not all, Ni/NiO_x particles. This implies the formation of a Ni−Cr mixed metal oxide, which is highly effective in water reduction. Inhomogeneities in the interfacial contact, evident from differences in contact angles between Ni/NiO_x particles and the Mg:$SrTiO_3$ semiconductor, likely affect the probability of reduction of Cr(VI) species during synthesis by photodeposition, explaining the observed inhomogeneity in the spatial CrO_x distribution. Furthermore, by comparison with undoped $SrTiO_3$, Mg-doping appears essential to provide such favorable interfacial contact and to establish the beneficial effect of CrO_x. This study suggests that the performance of semiconductors can be significantly improved if inhomogeneities in interfacial contact between semiconductors and highly effective catalytic nanoparticles can be resolved by (surface) doping and improved synthesis protocols.

KEYWORDS: *photocatalytic water splitting, co-catalyst, stability, in situ ICP-MS, $SrTiO_3$*

INTRODUCTION

The performance of $SrTiO_3$ (STO)-based photocatalysts in the light-driven overall splitting of water to H_2 and O_2 has recently been significantly improved by aliovalent doping of the perovskite material by Al or Mg, and surface modification by deposition of appropriate co-catalysts such as Rh/CrO_x.[1−7] Triggered by this successful development, the first large-scale flat-plate reactors are evaluated in long-term stability measurements under realistic conditions.[7] The outstanding properties of aliovalently doped Al:STO have been assigned to removal (lower density) of Ti^{3+} mid-gap states (favorable recombination sites), which was recently confirmed by a combined experimental and theoretical investigation.[4] Similarly, for Mg:STO composites (apparent quantum yield, AQY, of 10% promoted with Ni/NiO), some of us proposed that Mg reduces the density of free-charge carriers, leading to a favorable surface-space-charge layer, promoting the oxygen evolution reaction.[3] Still co-catalyst modification is mandatory to facilitate water reduction at the surface of these aliovalently doped $SrTiO_3$-based composites. Particularly, co-catalysts consisting of chromium oxide and typically Rh[8−10] have

Received: July 10, 2021
Revised: August 7, 2021
Published: August 20, 2021

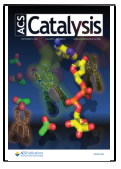

been widely utilized to induce photocatalytic activity of $SrTiO_3$ or Al:$SrTiO_3$ photocatalysts. In this context, CrO_x is generally proposed to form thin-film coatings on active hydrogen evolution catalysts, preventing the parasitic oxygen reduction reaction.[6,8,11−13] Despite the frequently employed picture of a core−shell structure, recent studies demonstrate that formation of mixed metal oxides containing CrO_x and, e.g., Rh, is also likely.[1,14,15]

Ni/NiO co-catalysts are another type of often employed co-catalysts enabling photocatalytic overall water splitting. Similarly to CrO_x in Rh/CrO_x, a NiO-shell is believed to prevent oxygen reduction to occur on the metallic Ni core.[16] Additionally, it has been reported that spatially separated particles of Ni and NiO_x promote the formation of hydrogen and oxygen, respectively.[17,18] Recently, some of us revealed significant and unfavorable transients in the hydrogen production rate using Ni/NiO-modified $SrTiO_3$.[18] Dynamics in composition and structure of the Ni/NiO core−shell particles correlate well with the observed transients in gas evolution.[19] Apparently, stabilization of the active phase(s) of the Ni/NiO co-catalyst system is required to fully exploit the potential of the system, which is potentially more economically viable than Rh-based formulas.[19−21]

Here, we report a novel insight into the extent and origin of the effect of CrO_x prepared by reductive photodeposition and Mg used as aliovalent dopant of $SrTiO_3$ on the unprecedented enhancement of the photocatalytic stability of Ni/NiO_x-Mg:$SrTiO_x$ composite photocatalysts. High-resolution transmission electron microscopy with energy-dispersive X-ray or electron energy-loss spectroscopy (HRTEM-EDX/EELS) reveals a spatial CrO_x distribution primarily in the vicinity of the Ni/NiO_x particles. The EDX and EELS data are explained by the formation of mixed CrO_x/NiO_x phases. Moreover, (*in situ*) inductively coupled plasma mass spectrometry/optical emission spectrometry (ICP-MS/OES) illustrates a significant reduction in leaching/dissolution of Ni ions from CrO_x/NiO_x phases compared to Ni/NiO_x during cyclic operation. Based on the presented results, it will be discussed that Mg synergistically promotes the activity of the composite photocatalyst, likely by providing a favorable interfacial contact between the semiconductor (Mg:$SrTiO_3$) and the Ni/NiO_x particles, enabling the inclusion of CrO_x by photodeposition. The insights provided will guide research devoted to increasing stability and overall performance of photocatalysts.

EXPERIMENTAL METHODS

Materials. $SrTiO_3$ was prepared by mixing and grinding of stoichiometric amounts of $SrCO_3$ (99.995% Sigma-Aldrich) and Rutile TiO_2 (99.995% Sigma-Aldrich) and subsequent calcination at 1100 °C for 10 h. Mg:$SrTiO_3$ was prepared following a two-step procedure. A detailed description of the experimental procedure and additional characterization is provided elsewhere.[3] Briefly, $MgSO_4$ was mixed with Rutile (TiO_2) and treated at 800 °C in air. Obtained powders were converted to Mg:$SrTiO_3$ by mixing and grinding with $SrCO_3$ and calcination at 1100 °C for 10 h. Remaining sulfate was removed by thorough washing.[3] The ratio of materials was adjusted to enable synthesis of an Sr(Mg,Ti)O_3 compound with a composition of $Sr_{1.25}Mg_{0.3}Ti_1O_x$. Here, magnesium (ionic radius of Mg^{2+} 72 pm) is expected to be at the B-site of the ABO_3-perovskite, being in agreement with similarities in ionic radius (74 pm Ti^{4+}). Hereafter, the Mg-modified $SrTiO_3$ is identified by Mg:$SrTiO_3$.[3] Detailed characterization (see also the Results and Discussion section on HRTEM/EDX and ICP analysis) shows that the actual Mg content is lower in the active Mg:$SrTiO_3$ composite. This is caused by significant dissolution of Mg upon suspension in water, needed for washing, Ni impregnation, and photodeposition of CrO_x (see also the Results and Discussion section on *ex situ* ICP analysis).

To deposit core/shell-type Ni/NiO co-catalysts,[19] 0.2 g of Mg:$SrTiO_3$ or $SrTiO_3$ was dispersed in 20 mL of an aqueous solution of $Ni(NO_3)_2$. The obtained mixture was stirred for 2 h, and afterward, the solution was evaporated till dryness (80 °C, overnight). The Ni precursor was converted to NiO at 400 °C (10 K min^{-1} ramp rate) in synthetic air (30 mL min^{-1}), followed by treatment in 5% H_2/N_2 (80 mL min^{-1}) at 500 °C (at 10 K min^{-1}) for 10 h. Core/shell Ni/NiO structures were obtained by cooling the tube furnace to 130 °C in N_2 (80 mL min^{-1}), before introducing N_2 and subsequently air (30 mL min^{-1}) for 1 h. The Ni loading was verified to be 1 wt % by X-ray fluorescence (XRF) analysis.

Modification with chromium oxide was achieved by photodeposition. Briefly, 0.1 g of Ni/NiO_x-Mg:$SrTiO_3$ or Ni/NiO_x-$SrTiO_3$ was dispersed in 10 mL of a 10 mM $K_2Cr_2O_4$ solution (pH ∼ 5). The resulting slurry was illuminated for 3 h using a UV light-emitting diode (LED) light source (365 nm, 3.2 mW cm^{-2}). Afterward, the obtained powder was separated from solution by filtration and dried at 80 °C for 12 h. The amount of CrO_x, independent of the presence of Mg, was verified to be 0.2 wt % in all cases by X-ray fluorescence (XRF) analysis.

Photocatalytic Activity Experiments. The photocatalytic activity of the synthesized photocatalysts (25 mg catalyst in 25 mL deionized, DI water) was measured using a continuously stirred tank reactor (30 mL cuvette, 402.013-OG obtained from Hellma), equipped with a gas-tight lid.[22] Products were stripped from the reactor with a continuous He flow of 10 mL min^{-1}, unless otherwise specified, and analyzed using a gas chromatograph (GC) equipped with a highly sensitive Pulsed Discharge Detector (Interscience). Apparent quantum efficiencies were determined using 365 nm LED illumination (Roithner LaserTechnik), with a measured intensity of 1.9 mW cm^{-2}. The area of illumination was 2.25 cm^2 for all experiments and oxygen was removed from the solution prior to illumination by He purge overnight. Gas production rates are presented both as rates (μmol min^{-1}) and mass normalized rates (μmol g^{-1} min^{-1}) to allow for a comparison with the literature. It is, however, noted that there is likely no linear relation between production rates and photocatalyst mass.

Characterization. X-ray diffraction (XRD) measurements were performed with a Bruker D2 (Cu Kα source) Diffractometer. Raman spectroscopy was performed at room temperature using an Avantes AvaRaman spectrometer, equipped with a 785 nm laser. A Philips PW 1480 analyzer was used for XRF analysis. X-ray photoelectron spectroscopy (XPS) was measured using a Quantera SXM from Physical Electronics using monochromatic Al Kα radiation (1486.6 eV). All spectra were calibrated to the carbon C1s peak at 284.8 eV. Detailed TEM analysis was performed at different magnifications. Survey imaging of the fresh Ni/NiO-Mg:$SrTiO_3$ and CrO_x-modified Ni/NiO-Mg:$SrTiO_3$ was performed using a JEOL 2010F microscope, operating at 200 kV. Local elemental analysis was obtained from a probe-corrected JEOL ARM200F scanning TEM (STEM), operating at 200 kV, equipped with a

https://doi.org/10.1021/acscatal.1c03104
ACS Catal. 2021, 11, 11049−11058

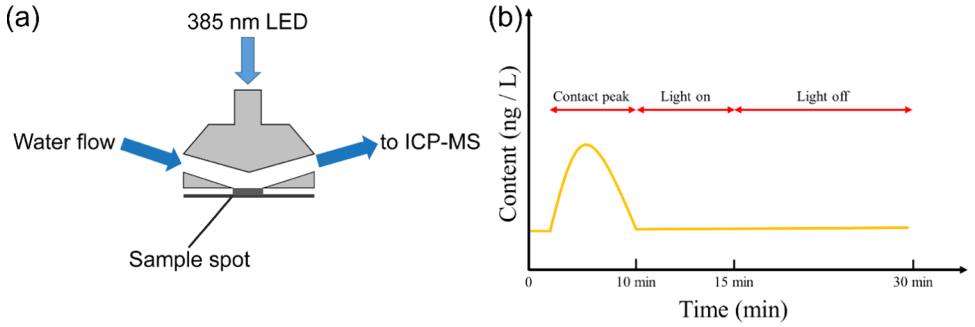

Figure 1. Schematic illustration of the applied ICP-MS measurement geometry (a) and the sequence of measurement (b). In (b), the peak width of about 10 min realistically represents the actual concentration profile.

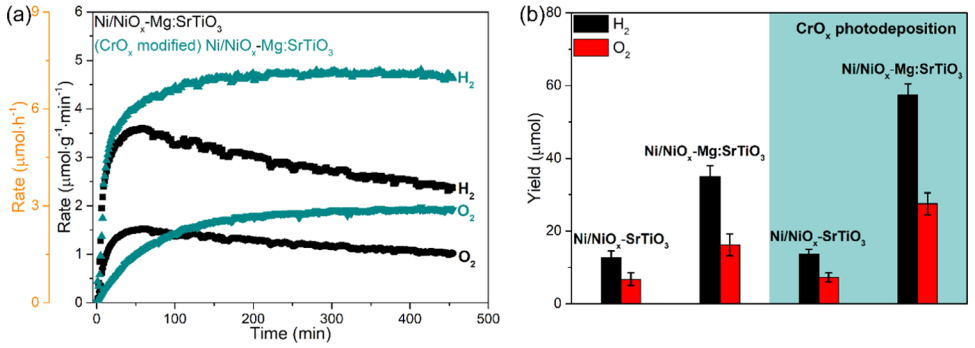

Figure 2. (a) Time-resolved photocatalytic water splitting performance of (CrO_x-modified) Ni/NiO_x-$Mg:SrTiO_3$ composites using 365 nm LED illumination. Reaction conditions: 25 mg of catalyst in 25 mL of DI water. (b) Hydrogen and oxygen yields of Ni/NiO_x-$SrTiO_3$ and Ni/NiO_x-$Mg:SrTiO_3$ in the absence and presence of CrO_x; constant illumination was applied for a period of 8 h. Reaction conditions: 25 mg of catalyst in 25 mL of DI water using 365 nm LED light.

windowless EDAX X-ray detector and a Gatan Enfinium EELS spectrometer. High-resolution TEM (HRTEM) imaging at 300 kV was performed with an aberration-corrected FEI Titan instrument.

In situ ICP-MS measurements were performed in a photoelectrochemical scanning flow cell (SFC) connected to an inductively coupled plasma mass spectrometer (ICP-MS) (NexION 300X, PerkinElmer).[23] Daily calibration was performed with a four-point calibration at concentrations of (0; 0.5; 1; 5) $\mu g\ L^{-1}$ for Mg, Ti, Ni, Cr, and Sr with standard solutions (Merck Certipur) mixed in DI water (Merck Millipore). Sc(Mg, Ti), Co(Ni), and Y(Cr, Sr) solutions at 10 $\mu g\ L^{-1}$ in 1% HNO_3 were used as internal standards. Several photocatalysts (Ni/NiO_x-$SrTiO_3$, Ni/NiO_x-$Mg:SrTiO_3$, and CrO_x-modified Ni/NiO_x-$Mg:SrTiO_3$) were immobilized by drop-casting from aqueous suspension on glassy carbon substrates. The loading of every individual measurement spot was ~15 μg and a spot size of around 1.2 mm was used (Figure 1).[23−25] A flow of liquid DI water of 186 $\mu L\ min^{-1}$ was introduced, and the water composition was analyzed after contact with the sample. The flow was maintained for 10 min in darkness, after which the photocatalyst was exposed to light (385 nm, 60 mW cm^{-2}, Thorlabs M385F1) for 5 min. Finally, the water flow was maintained for an additional 15 min in the dark. The Sr, Ti, Mg, and Ni-contents in the effluent were analyzed by integration over the various treatment periods (light on/off). Additionally, ICP-OES analysis (*ex situ*) of liquid aliquots taken during activity measurements were performed using a PerkinElmer 8300dv to determine concentrations of dissolved Cr, Mg, and Ni at different stages of the reaction. Prior to the ICP-OES analysis, the photocatalyst was isolated from the slurry solution by filtration, and only isolated clear solutions were used for analysis.

RESULTS AND DISCUSSION

Performance Evaluation: Overall Water Splitting and Back Reaction. The photocatalytic water splitting activities induced by UV light illumination (365 nm LED source) of $Mg:SrTiO_3$ with either Ni/NiO_x or CrO_x-modified Ni/NiO_x co-catalysts are compared in Figure 2a.

The initial rapid increase in apparent gas production for both catalysts is due to the characteristic residence time of product gas in the reactor and feed-lines to the GC, and the time needed to reach steady state as usually observed in continuously stirred tank reactors (CSTR). A decrease in gas production is observed for Ni/NiO_x-$Mg:SrTiO_3$ under continuous operation,[3,19] which we previously assigned to changes in oxidation state and morphology of the core/shell Ni/NiO particles in Ni/NiO_x-$SrTiO_3$. Remarkably, after CrO_x-modification the stability of the photocatalyst is significantly improved, retaining at least 90% of the steady-state photocatalytic activity after 70 h of day/night cyclic operation (8.4 $\mu mol\ h^{-1}$ or 5.6 $\mu mol\ g^{-1}\ min^{-1}$ of H_2 is produced; see Figure S1). Considering the measured photon flux of the 365 nm LED light, the apparent quantum yield (AQY) is calculated to be 26 ± 2% for CrO_x-modified Ni/NiO_x-$Mg:SrTiO_3$ (for data on simulated solar illumination, see Figure S2).

Figure 2b shows the effect of the presence of Mg-doping on the beneficial effect of photodeposition of CrO_x. Interestingly, CrO_x modification of Ni/NiO_x-$SrTiO_3$ hardly leads to improvement (the H_2 production yield obtained after 8 h

https://doi.org/10.1021/acscatal.1c03104
ACS Catal. 2021, 11, 11049−11058

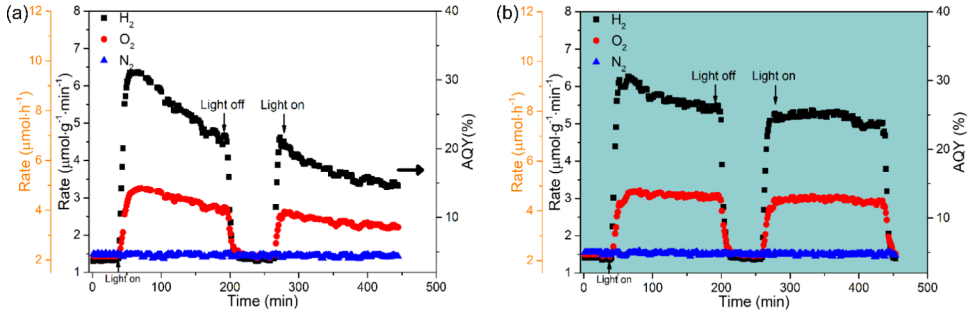

Figure 3. Photocatalytic activity of Ni/NiO_x-Mg:$SrTiO_3$ (a) and CrO_x-modified Ni/NiO_x-Mg:$SrTiO_3$ (b) composites when a mixture of H_2, O_2, and N_2 (all at 80 ppm) is used as purge gas. Reaction condition: 25 mg of catalyst in 25 mL of DI water with 365 nm LED as the light source.

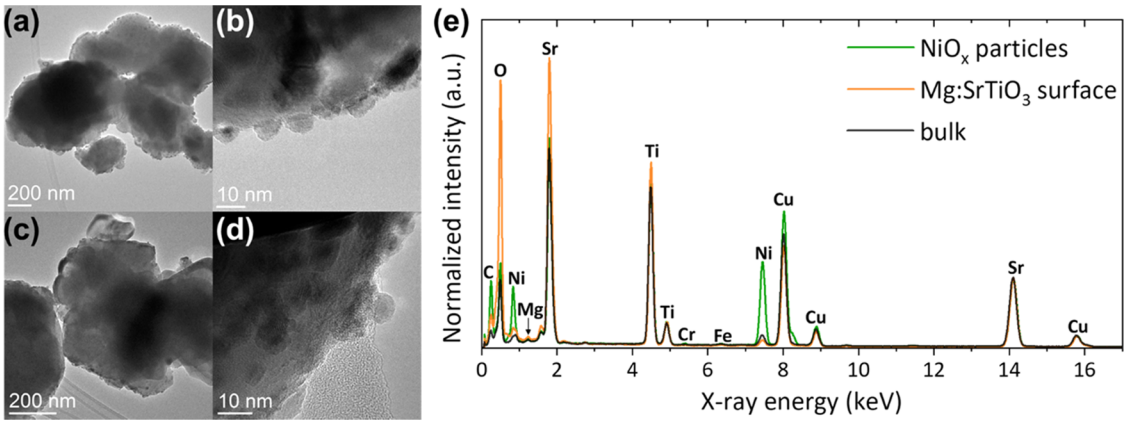

Figure 4. Survey TEM images of (a, b) fresh Ni/NiO_x-Mg:$SrTiO_3$ composite and (c, d) fresh CrO_x-modified Ni/NiO_x-Mg:$SrTiO_3$ composite. (e) Summed EDX spectra of the fresh CrO_x-modified Ni/NiO_x-Mg:$SrTiO_3$ composite: Black line indicates bulk, and green and orange lines indicate surface regions containing NiO_x particles and no particles, respectively. (The Cu signal arises from the Cu TEM support grid and is not part of the sample).

only increases from 510 to 550 μmol g^{-1}), while the steady-state performance of Ni/NiO_x-Mg:$SrTiO_3$ was improved by a factor of ~2 by photodeposition of CrO_x. In the absence of Mg, CrO_x furthermore has a significantly smaller positive effect on the stability (Figure S3). These observations suggest that Mg is essential to achieve the positive effect of CrO_x on the performance of Ni/NiO_x core/shell particles.[1,10]

In studies on photocatalytic water splitting, significant improvements in activity and selectivity due to CrO_x-modification are generally assigned to suppression of the unfavorable oxygen reduction reaction (ORR) by forming a protective shell around among others Rh nanoparticles.[26] Therefore, we determined the photocatalytic performance of the Mg-doped composites in the presence of exogenous oxygen (and hydrogen). In the absence of light, neither Ni/NiO_x-Mg:$SrTiO_3$ nor the CrO_x-modified Ni/NiO_x-Mg:$SrTiO_3$ photocatalyst induces (chemical) conversion of O_2. Figure 3 compares the characteristic photocatalytic performance (rate is displayed on the left *y*-axis and the AQY on the right *y*-axis) of (CrO_x-modified) Ni/NiO_x-Mg:$SrTiO_3$ when purging 80 ppm of H_2 and 80 ppm of O_2. Once initiating illumination, H_2 and O_2 are produced resembling the trends observed in pure He purge (compare Figure 2). Terminating illumination results in a fast transient in gas production, and concentrations quickly stabilize to the background levels. Reinitiating illumination recovers gas production, with Ni/NiO_x-Mg:$SrTiO_3$ continuing deactivation. Since the partial pressure of oxygen in continuous flow reactors is typically low in comparison to batch-type systems,[27−29] the absence of the oxygen reduction reaction (at 80 ppm) was to be expected.[10,30]

This is further confirmed by a transient in feed gas from He to the gas containing 80 ppm of H_2, O_2, and N_2 during a photocatalytic experiment (Figure S4), hardly showing any effect of this gas compositional change on performance. Finally, production rates of H_2 and O_2 are independent of the purge-gas flow rate (Figure S5),[27,29] which should not be the case if reduction of oxygen occurs.[29,31,32] Summarizing, these results show that Ni/NiO_x core−shell structures appear to be poor catalysts for the ORR at the concentrations relevant for the present study, and it is thus unlikely that suppression of unwanted side reactions by CrO_x deposition explains the enhanced stability and increased production rates of CrO_x promoted NiO_x-Mg:$SrTiO_3$.[10] Alternatively, we propose that a mixed oxide formulation of CrO_x and Ni/NiO_x (and Mg) is formed, which is highly effective in the water reduction reaction, and enhances the stability against dissolution of NiO_x phases. First, we will provide evidence for the formation of mixed Cr and Ni oxide phases, and will discuss the spatial distribution of CrO_x in the composite, followed by a detailed study of dissolution of NiO_x in the investigated catalytic formulations.

Materials Characterization: Localizing Photodeposited CrO_x. In an attempt to localize CrO_x on the surface of the prepared photocatalysts, XRD (Figure S6), Raman (Figure S7), XPS, and (HR/S)TEM were used. XRD, Raman, and XPS were not able to provide any evidence of the oxidation state, nor crystal structure of CrO_x and as such CrO_x appears to be

https://doi.org/10.1021/acscatal.1c03104
ACS Catal. 2021, 11, 11049−11058

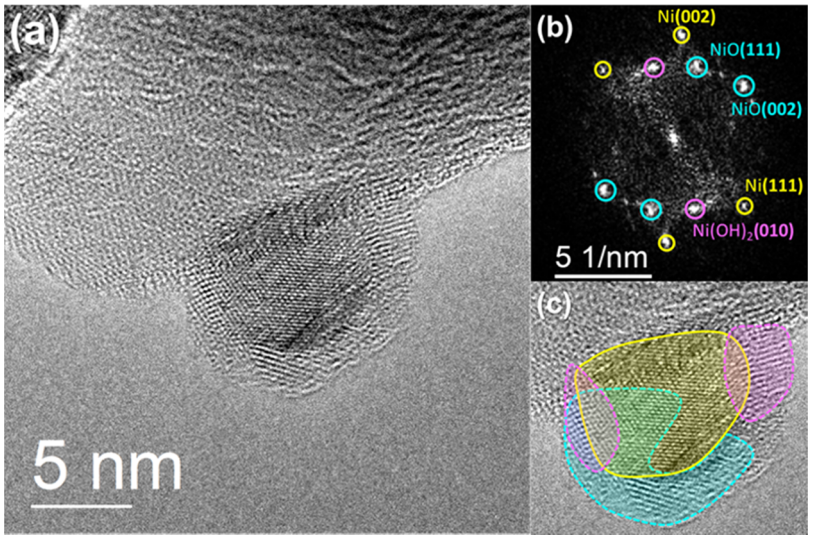

Figure 5. (a) HRTEM image of a typical Ni/NiO_x core−shell particle of CrO_x-modified Ni/NiO_x-Mg:$SrTiO_3$ with a low contact angle. Similar images were obtained for Ni/NiO_x-Mg:$SrTiO_3$ in the absence of CrO_x. (b) FFT from the region containing the supported core−shell particle with Ni, NiO, and $Ni(OH)_2$ lattice spacings identified. (c) Regions of the core−shell particle containing Ni (yellow), NiO (blue), and $Ni(OH)_2$ (pink) as identified using inverse FFTs of the individual diffraction spot pairs.

present in low quantities on the surface. It is also worthwhile to mention that reduced forms of Ti, such as Ti^{3+}, were not detected by means of XPS, potentially as a result of the performed reductive treatment used for Ni/NiO_x synthesis.

The oxidation states of the Ni/NiO_x co-catalyst on the surface of Ni/NiO_x-Mg:$SrTiO_3$ and CrO_x-modified Ni/NiO_x-Mg:$SrTiO_3$ were determined by XPS for both the as-prepared and measured samples. In as-prepared Ni/NiO_x-Mg:$SrTiO_3$ (Figure S8a) the Ni $2p_{3/2}$ signal mainly consists of contributions from Ni^{2+} (NiO at 853.5 eV). A minor contribution of metallic Ni^0 (851.9 eV) is also revealed. After illumination, the width and symmetry of the Ni signal change, which suggests that the relative contribution of Ni^{2+} (as in $Ni(OH)_2$ at 855.6 eV) is significantly enhanced compared to Ni^0. Formation of NiOOH might also contribute to the overall peak shape. This assignment is also in agreement with the changes in the O1s signal induced by illumination (Figure S9).[19] In contrast, Ni and O signals of the CrO_x-modified Ni/NiO_x-Mg:$SrTiO_3$ composite show little difference, before and after illumination (Figure S8b), suggesting that NiO_x preserves the oxidation state (Ni^{2+} (as in $Ni(OH)_2$ at 855.6 eV) and presumably some NiOOH). In fact the dominant presence of oxidized Ni-species in the as-prepared CrO_x-modified Ni/NiO_x-Mg:$SrTiO_3$ is likely due to the applied photodepostion procedure, in which the most stable Ni oxidation state was formed.

TEM images showing the morphology of the as-prepared photocatalysts are compared in Figure 4a−d. All materials exhibit large Mg:$SrTiO_3$ particles in the order of several hundreds of nanometers. Ni/NiO_x core−shell particles decorate the surface throughout and are roughly 5−30 nm in size with a shell thickness of approximately 2 nm (for HRTEM images of Ni/NiO_x particles, the reader is referred to Figures S10−S14). The morphology of the supported Ni/NiO_x core−shell particles is rather heterogeneous throughout each sample. Specifically, for some core−shell particles low contact angles (indicating good bonding to the support) are revealed, whereas weak interfaces with larger contact angles are observed for others.

To investigate differences in the structure of the Ni/NiO_x particles on each photocatalyst composite in more detail, both before and after undergoing photocatalytic measurements, HRTEM imaging was performed. Figure 5a shows a typical core−shell particle as observed for CrO_x-modified Ni/NiO_x-Mg:$SrTiO_3$, being almost indistinguishable from particles analyzed in (Cr-free) Ni/NiO_x-Mg:$SrTiO_3$ (see for comparison Figures S12 and S14). In Figure 5b, the corresponding fast Fourier transform (FFT) is displayed showing the presence of Ni, NiO, and $Ni(OH)_2$, in agreement with XPS analysis and previous observations reported for Ni/NiO_x-$SrTiO_3$ composites after illumination.[19] Thus, we suggest $Ni(OH)_2$ most likely forms as a result of illumination during photodeposition of CrO_x. Using inverse FFT analysis (Figure S9), the distribution of the different phases was explored and shows a clear Ni core surrounded primarily by NiO and smaller patches of $Ni(OH)_2$ (see Figure 5c, additional images are shown in Figures S11 and S13). Interestingly, no CrO_x overlayers were found surrounding any of the imaged Ni/NiO_x particles on both the as-prepared and used CrO_x-modified Ni/NiO_x-Mg:$SrTiO_3$. Nominally, there is no difference between the supported particles on either sample and particle growth that may result from the deposition of a CrO_x layer is absent.[13] Moreover, the Ni/NiO_x particles are barely distinguishable from that on Ni/NiO_x-Mg:$SrTiO_3$ (see Figures S12 and S14 for HRTEM images) suggesting the Cr incorporation is very subtle and may indeed be present in mixed oxide species.

To further examine the CrO_x-modified Ni/NiO_x-Mg:$SrTiO_3$ photocatalysts STEM was used and EDX and EELS (see Supporting Information Figure S15) spectra were collected from the surface and the bulk of the material. In total, fifteen regions over the surface containing Ni/NiO_x particles, ten areas of the Mg:$SrTiO_3$ surface without supported particles, and seven entire aggregates (i.e., bulk) were inspected by EDX. Due to the low Cr signal (and Mg) in each individual EDX spectra, the different groups of spectra were summed and are displayed in Figure 4e. In all summed EDX spectra, the Cr signal is weak while the Ni signal is expectedly strong at regions of the surface containing Ni/NiO_x particles. Consid-

https://doi.org/10.1021/acscatal.1c03104
ACS Catal. 2021, 11, 11049−11058

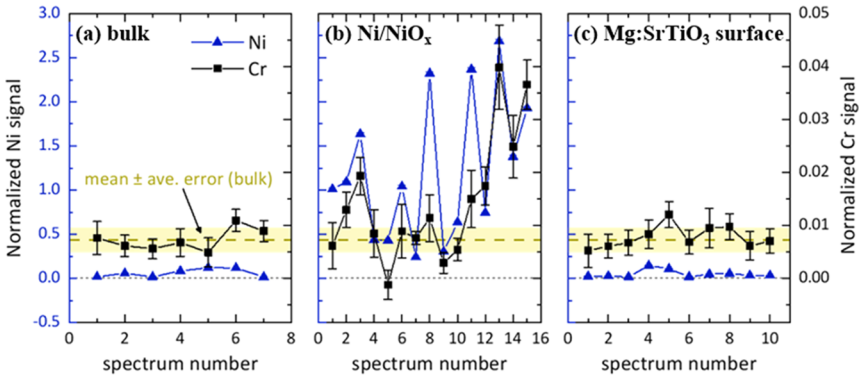

Figure 6. EDX signal analysis: Integrated and normalized Ni (left vertical axis, blue) and Cr (right vertical axis, black) signals determined in each individual spectrum from the bulk (a), supported NiO_x particles (b), and the bare Mg:$SrTiO_3$ surface (c). The mean and average error ($7.22 \times 10^{-2} \pm 2.37 \times 10^{-2}$) associated with the integrated Cr signal for the bulk, representing the pole piece fluorescence, is marked on each panel in gold/yellow.

ering that each spectrum contains a baseline Cr signal originating from constant objective lens pole piece excitation by X-rays emitted from the respective sample, Cr and Ni signals were normalized (for normalization procedure see Supporting Information). Figure 6 compares the integrated normalized Ni and Cr signals for EDX spectra collected from the bulk (Figure 6a), Ni/NiO_x particles (Figure 6b), and the Mg:$SrTiO_3$ surface (Figure 6c). In addition, the Cr/Fe ratio (i.e., a ratio of the normalized Cr and Fe signals) for all spectra is shown in Figure S16. In all spectra collected from regions containing Ni/NiO_x particles, the normalized Ni signal is about 3−40 times greater (left *y*-axis in Figure 6) than the average normalized Cr signal found in the bulk or at the bare Mg:$SrTiO_3$ surface (Figure 6, see also Supporting Information for additional information). Note that for clarity the baseline Cr signal attributed to the pole piece fluorescence, the mean and average error ($7.22 \times 10^{-2} \pm 2.37 \times 10^{-2}$) of the integrated Cr signal associated with the bulk measurements is plotted (yellow areas) on all three graphs.

For about half of the regions possessing Ni/NiO_x particles (i.e., spectra 2−3 and 11−15) also significant contributions of Cr were obtained. Interestingly, a very high Ni signal does not always correlate with a high Cr signal as revealed in spectra 8 and 11 (see Figure 6b and also Figure S17 comparing EDX data of spectra 8 and 15). Since roughly half of the Ni/NiO_x-containing particles (6 out of the 15 areas) contain additional Cr content beyond the background level, this implies that the photodeposition of CrO_x onto Ni/NiO_x has not been consistent nor homogeneous. Finally, the low integrated Cr signal (Figure 6c) and Cr/Fe ratios (Figure S16) from regions of the Mg:$SrTiO_3$ surface are similar to that of the bulk, which further supports that CrO_x was deposited preferentially onto several, likely specific Ni/NiO_x particles, rather than uniformly throughout the surface. In contrast, the Mg peak is equal in all summed spectra indicating a homogeneous distribution of Mg throughout the bulk and surface of the support particles (compare also Figure 4b). The amount of Mg incorporated into the particles is consistent with a composition of $Mg_{0.03}Sr_{1.25}TiO_3$ according to EDX simulations done with NIST's DTSA-II software (Figure S18).

One can draw a few interesting and summarizing conclusions from the characterization and especially the EDX analysis. First, a dramatic effect in photocatalytic efficiency is observed, despite the small amount of Cr present and the absence of a continuous CrO_x layer or coating. Likely a mixed-Ni−Cr oxide is formed on the nanoscale. Second, the heterogeneity of the Cr distribution and loading on the Ni/NiO_x suggests that there are vast opportunities for further improvement of photocatalyst. Specifically, an increase in performance can be expected by achieving a more uniform distribution of CrO_x in contact with the Ni/NiO_x particles. Two hypotheses can be proposed to explain the presence of CrO_x in the vicinity of some, and the absence of others. First, the revealed heterogeneity in CrO_x distribution may result from differences in the NiO_x shell thickness. Relatively thick shells (which are probably insulating) may prevent photogenerated electrons to transfer from the Mg:doped $SrTiO_3$ semiconductor to the deposited Ni/NiO_x particles, preventing reduction of Cr(VI)-ions in the photodeposition procedure. Conversely, any cracks within the NiO_x shell would expose the Ni metal and promote photodeposition. The consistent shell thickness and continuity of the NiO shells in several images, however, does not strongly support this hypothesis. Another explanation for inhomogeneity might be differences in the interfacial/electrical contact between the Ni/NiO particles and the Mg:$SrTiO_3$ support. Poor contact could also impede photodeposition from occurring. A similar effect has been observed on Ni/NiO core/shell structures on TiO_2 wherein the photocatalyst deactivates due to a photochemical reaction causing Ni to dissolve into solution.[20] In this case, only a fraction of the particles exhibited Ni leaching, which was believed to result from the good electrical contact between the light-absorbing TiO_2 support and Ni particles.[20] Several supported particles on the Mg:$SrTiO_3$ supports studied here were characterized by low contact angles (see Figures S10−S14), indicative of a strong interfacial contact that likely facilitates charge transport. Given the differences between Mg-doped and pure $SrTiO_3$ in photocatalytic activity[l], we suggest that the desired interfacial contact might also require the presence of surface Mg-ions. As such it even seems likely that a poor electrical interfacial contact between the Ni particles and the perovskite support will not only limit the photodeposition of CrO_x but will also limit the water splitting activity. Considering the heterogeneous nature of the materials, dedicated sample preparation is required to disentangle the phenomena and to provide final proof to support our hypothesis. Still improved catalyst preparation techniques aimed at establishing excellent contact between Ni/NiO_x and (doped) $SrTiO_3$ phases, may result in further enhancement of the photocatalytic activity.

https://doi.org/10.1021/acscatal.1c03104
ACS Catal. 2021, 11, 11049−11058

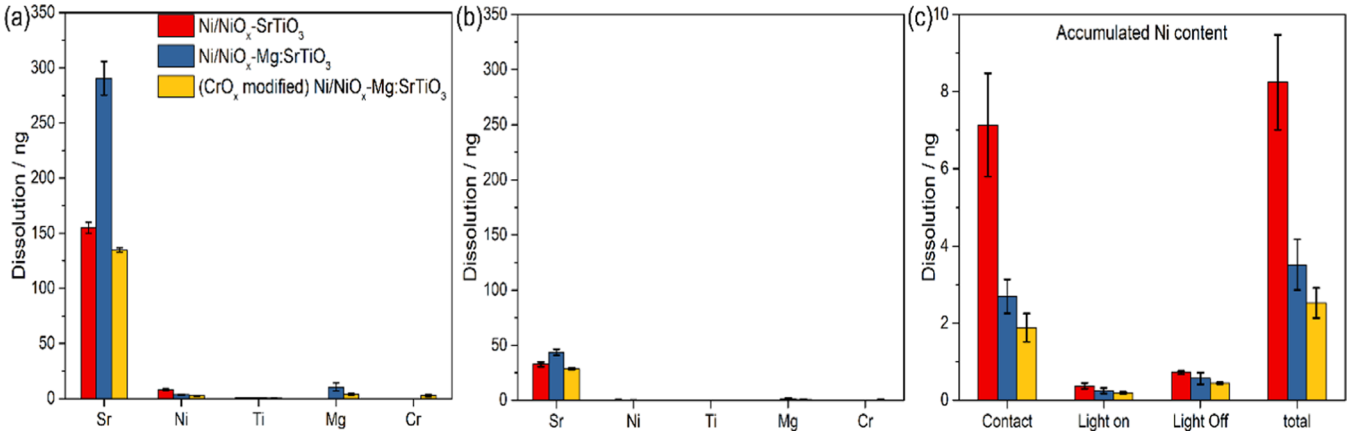

Figure 7. (a) *In situ* ICP-MS results of accumulated liquid content after 30 min of exposure to the photocatalyst, consisting of an initial 10 min of aqueous flow in darkness, illumination for 5 min, and additional aqueous flow for 15 min in darkness. (b) Accumulated amounts during 5 min of constant illumination. (c) Accumulated Ni-content [note the different scale compared to (a)] after 10 min of liquid flow ("contact"), 5 min of illumination ("light on"), 15 min of continuous flow ("light off"), and the accumulated total after 30 min. Measurement conditions: 15 μg per catalyst and 186 μL/min of water flow.

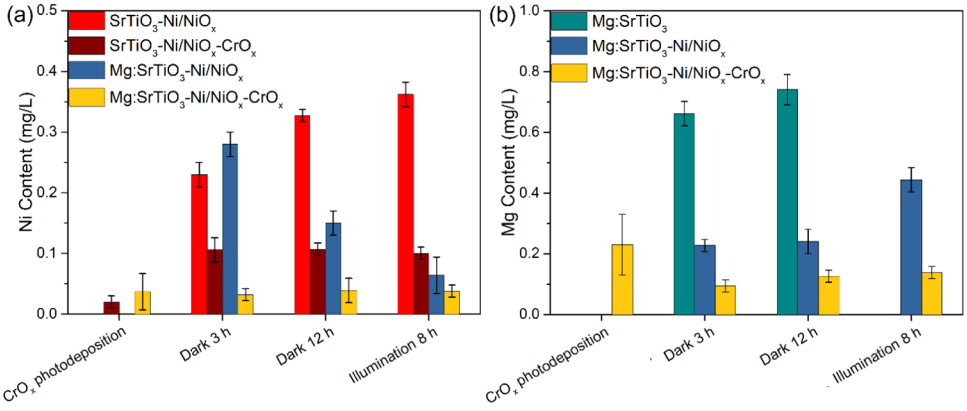

Figure 8. *Ex situ* ICP-OES analysis performed at different stages of a typical photocatalytic water splitting experiment: (a) Ni and (b) Mg contents. Reaction condition: 25 mg of catalyst in 25 mL of DI water. For each individual measurement, solution was extracted from the reactor and filtered to remove photocatalyst particles.

Accessing Photocatalyst Stability. We will now address the beneficial effect of CrO_x on the stability of the catalyst. Sophisticated *in situ* ICP-MS analysis of dissolution of various elements is therefore required,[21,28,33] and was combined with *ex situ* analyses.[23,25] Three different photocatalysts were analyzed by *in situ* ICP-MS, namely, Ni/NiO$_x$-SrTiO$_3$, Ni/NiO$_x$-Mg:SrTiO$_3$, and CrO$_x$-modified Ni/NiO$_x$-Mg:SrTiO$_3$, to understand the influence of Mg and CrO_x in more detail. These are shown in Figure 7.

It is immediately evident that Sr leaches rapidly from all samples (Figure 7a). In fact, rapid leaching occurs primarily upon contacting with water (Figures S19 and S20). Interestingly, Sr dissolution is most significant for Ni/NiO$_x$-Mg:SrTiO$_3$, suggesting that the presence of Mg promotes formation of an unstable surface structure associated with the A-site deficient perovskite. After photodeposition of CrO_x, the quantity of Sr dissolution from Ni/NiO$_x$-Mg:SrTiO$_3$ is reduced significantly. The fraction of Sr accumulated in 5 min of illumination at 385 nm is comparatively small (Figure 7b), and the relative amounts for the three investigated semiconductor composites are similar compared to the total accumulated amount of dissolved Sr. Detected quantities of Cr, Ni, and Mg were comparatively low and no Ti was detected for all photocatalyst composites tested. Similarly to Sr dissolution, Mg leaching appeared to be reduced after photodeposition of CrO_x. It is important to emphasize that initiating and terminating illumination did not result in significant transients in Sr dissolution or other elements.

Figure 7c summarizes dissolution of Ni. Dissolution of Ni is rapid and predominant in the first 10 min of aqueous flow (dark). Interestingly, dissolution of Ni is significantly lower for Mg-containing photocatalysts compared to Ni/NiO$_x$-modified SrTiO$_3$ (stoichiometric), suggesting that Mg stabilizes the interaction of Ni/NiO$_x$ with the surface of the semiconductor, in agreement with the previously discussed electron microscopy data. The addition of CrO_x appears to further enhance Ni stability against leaching, although it is important to emphasize that leaching of the most unstable Ni particles might have also occurred during the CrO_x-photodeposition procedure.

The results obtained by *in situ* ICP-MS regarding Ni dissolution are supported by *ex situ* ICP-OES analysis of the filtered solutions obtained at different times of activity testing (Figure 8). Though the overall amount of dissolved material is still low, again the largest quantities of dissolved Ni were determined for Ni/NiO$_x$-SrTiO$_3$. Interestingly, during testing of Ni/NiO$_x$-Mg:SrTiO$_3$, Ni^{2+} quantities in solution decreased after 12 h and further after 8 h of illumination in comparison to treatment for 3 h, suggesting that some Ni^{2+} is redeposited/

https://doi.org/10.1021/acscatal.1c03104
ACS Catal. 2021, 11, 11049−11058

adsorbed by prolonged exposure of this photocatalyst to water in the absence or presence of light.

During illumination, the determined quantity of dissolved Ni is significantly lower compared to the initial phases of testing, i.e., reactor purging before illumination (Figure 8a, blue bars). For all CrO_x-modified photocatalysts, leaching of Ni is clearly less pronounced and appeared to be constant already after 3 h of exposure to the solution while purging (brown and yellow bars in Figure 8a). Ni leaching is even further suppressed for Mg-containing Mg:$SrTiO_3$ materials (yellow bars). Focusing on the Mg content in the solution, the presence of Ni/NiO_x suppressed Mg dissolution (compare green and blue bars in Figure 8b). Addition of CrO_x further suppresses Mg leaching, which is otherwise most significant after illumination (after measurement).

Summarizing, *in situ* and *ex situ* ICP analyses show that: (i) Sr leaching is significant for $SrTiO_3$ and even more so for Mg:$SrTiO_3$, (ii) Mg is also found in solution, of which the quantity is smaller after photodeposition of CrO_x, (iii) leaching of Ni is significantly smaller for Mg-containing $SrTiO_3$, and (iv) photodeposition of CrO_x further reduces leaching of Ni/NiO_x.

Considering these results and the provided TEM analysis, we propose that mixed metal oxides are formed, i.e., containing Ni and Cr, likely anchored with low contact angles on surfaces terminated by Mg-containing crystal orientations. The establishment of such conformations is likely a function of leaching and redeposition phenomena occurring during photodeposition. Certainly, the implications of dissolution on the performance and stability of photocatalysts used for overall water splitting (or CO_2 reduction) in aqueous media are significant and of great importance to guide material development and industrial applicability of photocatalysts.

CONCLUSIONS

This work demonstrates, using state-of-the-art high-resolution microscopy and (*in situ*) elemental ICP analysis to follow metal dissolution, that stability of complex heterogeneous photocatalysts can be improved by additives, only present in traces. We have demonstrated that active co-catalyst phases of Cr and Ni are likely formed, preferably at locations with low contact angles between Ni/NiO_x core−shell particles and the Mg:$SrTiO_3$ surface, allowing effective charge transfer during the photodeposition procedure of CrO_x. Stability metrices such as metal dissolution are proposed here to be implemented in ongoing research to find efficient and durable photocatalysts to drive overall water splitting.

ASSOCIATED CONTENT

Supporting Information

The Supporting Information is available free of charge at https://pubs.acs.org/doi/10.1021/acscatal.1c03104.

Additional photocatalytic activity and stability data (Figures S1−S4); Raman, XRD, and XPS analyses (Figures S5−S8); HRTEM images (Figures S9−S13); STEM-EELS (Figure S14); and STEM-EDX (Figures S15−S17) results (PDF)

AUTHOR INFORMATION

Corresponding Authors

Guido Mul − *Faculty of Science & Technology, University of Twente, 7500 AE Enschede, The Netherlands;* orcid.org/0000-0001-5898-6384; Email: g.mul@utwente.nl

Bastian Mei − *Faculty of Science & Technology, University of Twente, 7500 AE Enschede, The Netherlands;* orcid.org/0000-0002-3973-9254; Email: b.t.mei@utwente.nl

Authors

Kai Han − *Faculty of Science & Technology, University of Twente, 7500 AE Enschede, The Netherlands;* Present Address: Inorganic Chemistry and Catalysis, Debye Institute for Nanomaterials Science, Utrecht University, 3854 CG Utrecht, The Netherlands

Diane M. Haiber − *School for Engineering—Matter Transport & Energy, Arizona State University, Tempe, Arizona 85287, United States;* orcid.org/0000-0002-8894-2144

Julius Knöppel − *Helmholtz Institute Erlangen-Nürnberg for Renewable Energy (IEK-11), Forschungszentrum Jülich GmbH, 91058 Erlangen, Germany; Department of Chemical and Biological Engineering, Friedrich-Alexander-Universität Erlangen-Nürnberg, 91058 Erlangen, Germany;* orcid.org/0000-0001-8355-3062

Caroline Lievens − *Faculty of Geo-information Science and Earth Observation, University of Twente, 7500 AE Enschede, The Netherlands*

Serhiy Cherevko − *Helmholtz Institute Erlangen-Nürnberg for Renewable Energy (IEK-11), Forschungszentrum Jülich GmbH, 91058 Erlangen, Germany;* orcid.org/0000-0002-7188-4857

Peter Crozier − *School for Engineering—Matter Transport & Energy, Arizona State University, Tempe, Arizona 85287, United States;* orcid.org/0000-0002-1837-2481

Complete contact information is available at: https://pubs.acs.org/10.1021/acscatal.1c03104

Author Contributions

K.H. and D.M.H. contributed equally to this work. The manuscript was written through contributions of all authors. All authors have given approval to the final version of the manuscript.

Funding

The China Scholarship Council is gratefully acknowledged for financially supporting K.H.

Notes

The authors declare no competing financial interest.

ACKNOWLEDGMENTS

T.L.M. Velthuizen is acknowledged for assistance with XRF analysis and the Catalytic Process Materials group at the University of Twente for providing access to the XRF equipment. Haiber (D.M.H.) and P. Crozier (P.C.) gratefully acknowledge the financial support from the U.S. Department of Energy (DE-SC0004954), the John M. Cowley Center for High Resolution Electron Microscopy, and the Eyring Materials Center. D.M.H. and P.C. also acknowledge assistance from Dr. Barnaby Levin for performing DTSA EDX simulation and assistance and discussion of STEM analysis.

ABBREVIATIONS

XRD, X-ray diffraction; XPS, X-ray photoelectron spectroscopy; TEM, transmission electron microscopy; EDX, energy-dispersive X-ray spectroscopy; ICP, inductively coupled plasma; MS, mass spectrometry; OES, optical emission spectrometry

REFERENCES

(1) Chiang, T. H.; Lyu, H.; Hisatomi, T.; Goto, Y.; Takata, T.; Katayama, M.; Minegishi, T.; Domen, K. Efficient Photocatalytic Water Splitting Using Al-Doped $SrTiO_3$ Coloaded with Molybdenum Oxide and Rhodium−Chromium Oxide. *ACS Catal.* **2018**, *8*, 2782−2788.

(2) Lyu, H.; Hisatomi, T.; Goto, Y.; Yoshida, M.; Higashi, T.; Katayama, M.; Takata, T.; Minegishi, T.; Nishiyama, H.; Yamada, T.; Sakata, Y.; Asakura, K.; Domen, K. An Al-Doped $SrTiO_3$ Photocatalyst Maintaining Sunlight-Driven Overall Water Splitting Activity for over 1000 h of Constant Illumination. *Chem. Sci.* **2019**, *10*, 3196−3201.

(3) Han, K.; Lin, Y.-C.; Yang, C.-M.; Jong, R.; Mul, G.; Mei, B. Promoting Photocatalytic Overall Water Splitting by Controlled Magnesium Incorporation in $SrTiO_3$ Photocatalysts. *ChemSusChem* **2017**, *10*, 4510−4516.

(4) Zhao, Z.; Goncalves, R. V.; Barman, S. K.; Willard, E. J.; Byle, E.; Perry, R.; Wu, Z.; Huda, M. N.; Moulé, A. J.; Osterloh, F. E. Electronic Structure Basis for Enhanced Overall Water Splitting Photocatalysis with Aluminum Doped $SrTiO_3$ in Natural Sunlight. *Energy Environ. Sci.* **2019**, *12*, 1385−1395.

(5) Ham, Y.; Hisatomi, T.; Goto, Y.; Moriya, Y.; Sakata, Y.; Yamakata, A.; Kubota, J.; Domen, K. Flux-Mediated Doping of SrTiO3 Photocatalysts for Efficient Overall Water Splitting. *J. Mater. Chem. A* **2016**, *5*, 3027−3033.

(6) Takata, T.; Jiang, J.; Sakata, Y.; Nakabayashi, M.; Shibata, N.; Nandal, V.; Seki, K.; Hisatomi, T.; Domen, K. Photocatalytic Water Splitting with a Quantum Efficiency of Almost Unity. *Nature* **2020**, *581*, 411−414.

(7) Goto, Y.; Hisatomi, T.; Wang, Q.; Higashi, T.; Ishikiriyama, K.; Maeda, T.; Sakata, Y.; Okunaka, S.; Tokudome, H.; Katayama, M.; Akiyama, S.; Nishiyama, H.; Inoue, Y.; Takewaki, T.; Setoyama, T.; Minegishi, T.; Takata, T.; Yamada, T.; Domen, K. A Particulate Photocatalyst Water-Splitting Panel for Large-Scale Solar Hydrogen Generation. *Joule* **2018**, *2*, 509−520.

(8) Chen, S.; Takata, T.; Domen, K. Particulate Photocatalysts for Overall Water Splitting. *Nat. Rev. Mater.* **2017**, *2*, No. 17050.

(9) Busser, G. W.; Mei, B.; Pougin, A.; Strunk, J.; Gutkowski, R.; Schuhmann, W.; Willinger, M.-G.; Schlögl, R.; Muhler, M. Photodeposition of Copper and Chromia on Gallium Oxide: The Role of Co-Catalysts in Photocatalytic Water Splitting. *ChemSusChem* **2014**, *7*, 1030−1034.

(10) Busser, G. W.; Mei, B.; Weide, P.; Vesborg, P. C. K.; Stührenberg, K.; Bauer, M.; Huang, X.; Willinger, M.-G.; Chorkendorff, I.; Schlögl, R.; Muhler, M. Cocatalyst Designing: A Regenerable Molybdenum-Containing Ternary Cocatalyst System for Efficient Photocatalytic Water Splitting. *ACS Catal.* **2015**, *5*, 5530−5539.

(11) Hisatomi, T.; Domen, K. Reaction Systems for Solar Hydrogen Production via Water Splitting with Particulate Semiconductor Photocatalysts. *Nat. Catal.* **2019**, *2*, 387−399.

(12) Maeda, K.; Teramura, K.; Lu, D.; Takata, T.; Saito, N.; Inoue, Y.; Domen, K. Photocatalyst Releasing Hydrogen from Water. *Nature* **2006**, *440*, 295.

(13) Maeda, K.; Teramura, K.; Lu, D.; Saito, N.; Inoue, Y.; Domen, K. Roles of Rh/Cr_2O_3 (Core/Shell) Nanoparticles Photodeposited on Visible-Light-Responsive $(Ga_{1-x}Zn_x)(N_{1-x}O_x)$ Solid Solutions in Photocatalytic Overall Water Splitting. *J. Phys. Chem. C* **2007**, *111*, 7554−7560.

(14) Kanazawa, T.; Maeda, K. Light-Induced Synthesis of Heterojunctioned Nanoparticles on a Semiconductor as Durable Cocatalysts for Hydrogen Evolution. *ACS Appl. Mater. Interfaces* **2016**, *8*, 7165−7172.

(15) Kurashige, W.; Mori, Y.; Ozaki, S.; Kawachi, M.; Hossain, S.; Kawawaki, T.; Shearer, C. J.; Iwase, A.; Metha, G. F.; Yamazoe, S.; Kudo, A.; Negishi, Y. Activation of Water-Splitting Photocatalysts by Loading with Ultrafine Rh−Cr Mixed-Oxide Cocatalyst Nanoparticles. *Angew. Chem., Int. Ed.* **2020**, *59*, 7076−7082.

(16) Domen, K.; Kudo, A.; Onishi, T.; Kosugi, N.; Kuroda, H. Photocatalytic Decomposition of Water into H_2 and O_2 over NiO-$SrTiO_3$ Powder. 1. Structure. *J. Phys. Chem. A* **1986**, *90*, 292−295.

(17) Townsend, T. K.; Browning, N. D.; Osterloh, F. E. Nanoscale Strontium Titanate Photocatalysts for Overall Water Splitting. *ACS Nano* **2012**, *6*, 7420−7426.

(18) Townsend, T. K.; Browning, N. D.; Osterloh, F. E. Overall Photocatalytic Water Splitting with NiO_x−$SrTiO_3$ − a Revised Mechanism. *Energy Environ. Sci.* **2012**, *5*, 9543−9550.

(19) Han, K.; Kreuger, T.; Mei, B.; Mul, G. Transient Behavior of Ni@NiO_x Functionalized $SrTiO_3$ in Overall Water Splitting. *ACS Catal.* **2017**, *7*, 1610−1614.

(20) Zhang, L.; Liu, Q.; Aoki, T.; Crozier, P. A. Structural Evolution during Photocorrosion of Ni/NiO Core/Shell Cocatalyst on TiO2. *J. Phys. Chem. C* **2015**, *119*, 7207−7214.

(21) Maeda, K.; Sakamoto, N.; Ikeda, T.; Ohtsuka, H.; Xiong, A.; Lu, D.; Kanehara, M.; Teranishi, T.; Domen, K. Preparation of Core-Shell-Structured Nanoparticles (with a Noble-Metal or Metal Oxide Core and a Chromia Shell) and Their Application in Water Splitting by Means of Visible Light. *Chem. - Eur. J.* **2010**, *16*, 7750−7759.

(22) Zoontjes, M. G. C.; Han, K.; Huijben, M.; van der Wiel, W. G.; Mul, G. The Effect of $Rh^{\delta+}$ Dopant in $SrTiO_3$ on the Active Oxidation State of Co-Catalytic Pt Nanoparticles in Overall Water Splitting. *Catal. Sci. Technol.* **2016**, *6*, 7793−7799.

(23) Knöppel, J.; Zhang, S.; Speck, F. D.; Mayrhofer, K. J. J.; Scheu, C.; Cherevko, S. Time-Resolved Analysis of Dissolution Phenomena in Photoelectrochemistry—A Case Study of WO_3 Photocorrosion. *Electrochem. Commun.* **2018**, *96*, 53−56.

(24) Klemm, S. O.; Topalov, A. A.; Laska, C. A.; Mayrhofer, K. J. J. Coupling of a High Throughput Microelectrochemical Cell with Online Multielemental Trace Analysis by ICP-MS. *Electrochem. Commun.* **2011**, *13*, 1533−1535.

(25) Zhang, S.; Rohloff, M.; Kasian, O.; Mingers, A. M.; Mayrhofer, K. J. J.; Fischer, A.; Scheu, C.; Cherevko, S. Dissolution of $BiVO_4$ Photoanodes Revealed by Time-Resolved Measurements under Photoelectrochemical Conditions. *J. Phys. Chem. C* **2019**, *123*, 23410−23418.

(26) Maeda, K.; Teramura, K.; Lu, D.; Saito, N.; Inoue, Y.; Domen, K. Noble-Metal/Cr_2O_3 Core/Shell Nanoparticles as a Cocatalyst for Photocatalytic Overall Water Splitting. *Angew. Chem., Int. Ed.* **2006**, *45*, 7806−7809.

(27) Fabian, D. M.; Hu, S.; Singh, N.; Houle, F.; Hisatomi, T.; Domen, K.; Osterloh, F. E.; Ardo, S. Particle Suspension Reactors and Materials for Solar-Driven Water Splitting. *Energy Environ. Sci.* **2015**, *8*, 2825−2850.

(28) Mei, B.; Han, K.; Mul, G. Driving Surface Redox Reactions in Heterogeneous Photocatalysis: The Active State of Illuminated Semiconductor-Supported Nanoparticles during Overall Water-Splitting. *ACS Catal.* **2018**, *8*, 9154−9164.

(29) Takanabe, K. Addressing Fundamental Experimental Aspects of Photocatalysis Studies. *J. Catal.* **2019**, *370*, 480−484.

(30) Dionigi, F.; Vesborg, P. C. K.; Pedersen, T.; Hansen, O.; Dahl, S.; Xiong, A.; Maeda, K.; Domen, K.; Chorkendorff, I. Suppression of the Water Splitting Back Reaction on GaN:ZnO Photocatalysts Loaded with Core/Shell Cocatalysts, Investigated Using a μ-Reactor. *J. Catal.* **2012**, *292*, 26−31.

(31) Takanabe, K. Photocatalytic Water Splitting: Quantitative Approaches toward Photocatalyst by Design. *ACS Catal.* **2017**, *7*, 8006−8022.

(32) Qureshi, M.; Takanabe, K. Insights on Measuring and Reporting Heterogeneous Photocatalysis: Efficiency Definitions and Setup Examples. *Chem. Mater.* **2017**, *29*, 158−167.

https://doi.org/10.1021/acscatal.1c03104
ACS Catal. 2021, 11, 11049−11058

(33) Spanu, D.; Minguzzi, A.; Recchia, S.; Shahvardanfard, F.; Tomanec, O.; Zboril, R.; Schmuki, P.; Ghigna, P.; Altomare, M. An Operando X-Ray Absorption Spectroscopy Study of a NiCu−TiO_2 Photocatalyst for H2 Evolution. *ACS Catal.* **2020**, *10*, 8293−8302.

https://doi.org/10.1021/acscatal.1c03104
ACS Catal. 2021, 11, 11049−11058